

FR II radio galaxies with $z < 0.3$ – I. Properties of jets, cores and hot spots

M.J. Hardcastle^{1,2*}, P. Alexander¹, G.G. Pooley¹ and J.M. Riley¹

¹ Mullard Radio Astronomy Observatory, Cavendish Laboratory, Madingley Road, Cambridge, CB3 0HE

² Department of Physics, University of Bristol, Royal Fort, Tyndall Avenue, Bristol BS8 1TL

6 October 2018

ABSTRACT

In previous papers we have discussed high-resolution observations of a large sample of powerful radio galaxies with $z < 0.3$. Jets are detected in up to 80 per cent of the sample, and radio cores in nearly all the objects; in addition, we are able to resolve the hot spots in most sources. In this paper we present measurements of the radio properties of these components.

The prominences of the jets detected do not appear to be a function of radio luminosity, providing the clearest evidence yet that the reported low detection rate of jets in radio galaxies has been an artefact of low-sensitivity observations. We find a positive correlation between the total source length and core prominence in the narrow-line radio galaxies. We have found evidence for a relationship between hot spot size and total source size, but few other significant relationships between hot spot properties and those of the jets or lobes. We compare our measurements to those of Bridle et al. (1994), based on observations of a sample of quasars, and argue that the results are consistent with a modification of the unified model in which the broad-line radio galaxies are the low-luminosity counterparts of quasars, although the situation is complicated by contamination with low-excitation radio galaxies which appear to have radio properties different from the high-excitation objects. We discuss the classes of empirical model that can be fitted to the dataset.

Key words: radio continuum: galaxies – galaxies: jets – galaxies: active

1 INTRODUCTION

Detailed images of classical double radio sources are essential if we are to understand the physics of such objects. In an earlier paper (Hardcastle et al. 1997; hereafter H97) we discussed high-resolution imaging of a sample of FRII (Fanaroff & Riley 1974) radio galaxies with $0.15 < z < 0.3$ drawn from the complete sample of Laing, Riley & Longair (1983; hereafter LRL). In this paper we combine this sample with the objects with $z < 0.15$ described in Black et al. (1992; hereafter B92) and Leahy et al. (1997; hereafter L97) to form a sample of 50 objects. High-resolution observations are available for almost all this combined sample, as described in B92, L97 and H97, and jets are detected in up to 80 per cent of the objects. In these earlier papers the properties of individual sources were discussed in detail. In the current paper we present and analyse systematic measurements made from these maps, particularly of the components (jets and cores) which directly relate to the energy transport in the sources, and investigate a number of trends and correlations in the data.

1.1 Unified models at $z < 0.3$

Unified models for classical double radio sources, in which the FRII radio galaxies are the parent population of radio-loud quasars (Scheuer 1987; Barthel 1987, 1989) are now widely accepted. The differences between the radio structures of radio galaxies and quasars are explained in terms of relativistic beaming of components of the sources (see section 1.2), while anisotropic obscuration explains the optical differences between them. Barthel (1989) showed that in the redshift range $0.5 < z < 1$ the relative numbers of quasars and radio galaxies in LRL, and their distributions of linear sizes, were consistent with every radio galaxy in the sample being a misaligned quasar.

However, a problem arises when applying the simplest version of the unified model to the sources at $z < 0.3$ considered in this paper. There are no FRII quasars in 3CR with $z < 0.15$ (Spinrad et al. 1985) or in LRL with $0.15 < z < 0.3$. These samples are selected on the basis of low-frequency flux density and so are thought to be free of orientation bias. If unified models are correct, the absence of quasars from the sample discussed here implies the presence in it of other objects aligned at a small angle to the line of sight

* Present address. E-mail *M.Hardcastle@bristol.ac.uk*

which should be detectable by anisotropic optical and radio emission. Barthel (1989) suggested that the broad-line radio galaxies (BLRG) were intermediate in viewing angle between quasars and the more common narrow-line radio galaxies (NLRG), which may be true in some cases; but in this sample at least the complete absence of lobe-dominated quasars makes it seem more likely that some or all of the objects classed as BLRG are true quasars whose optical continuum is insufficiently bright for them to be classed as such optically.[†] In this paper we shall test this model by comparing the radio properties of the BLRG in our sample to those of the NLRG and of powerful quasars.

The situation is rendered still more complicated by the presence in the sample of a number of low-excitation radio galaxies (LERG). This class of object was first discussed in Hine & Longair (1979); here we use the definition of Laing et al. (1994: hereafter L94). It is suggested (e.g. Barthel 1994) that these objects should not show broad emission lines whatever their angle to the line of sight, and that they form the parent population of BL Lac objects rather than core-dominated quasars; they will then certainly confuse any attempt to analyse orientation effects from radio data unless they are treated separately. If this is done carefully they should provide a valuable population for comparison with BLRG and NLRG if no other effects are present. However, we shall show that other effects do appear to be present in the sample discussed here.

In what follows we shall therefore discuss the overall properties of the sample with the emission-line classifications of the sources in mind. We shall compare the properties of this sample with those of others, particularly the high-resolution images of quasars in the similar study of Bridle et al. (1994; hereafter B94); the place of these objects in unified models should be borne in mind.

In the present sample there are 15 LERG, 9 BLRG and 25 NLRG. If the low-excitation objects are discarded, as discussed above, the proportion of BLRG to NLRG is consistent with the critical angle of 40–50° of Barthel (1989).

1.2 Relativistic beaming and radio source components

The emission from any component of the radio source moving at a significant fraction of the speed of light in the galaxy rest frame will be anisotropic. As seen on Earth, a feature with velocity $v = \beta c$ and Lorentz factor $\gamma = (1 - \beta^2)^{-\frac{1}{2}}$ has a flux density S_{obs} which can be related to the flux density it would have had at rest (S_{rest}) by the formula

$$S_{obs} = S_{rest}[\gamma(1 - \beta \cos \theta)]^{-(m+\alpha)} \quad (1)$$

(Ryle and Longair 1967) where θ is the angle made by the velocity vector with the line of sight, α is the spectral index (defined throughout in the sense $S \propto \nu^{-\alpha}$), and m is a

[†] It is important to realise that classifications in terms of broad or narrow lines are dependent on high-quality spectra, which are not in general available for this sample. Laing et al. (1994) have shown that the classifications can change significantly with improved observations. The classifications used here must be viewed as best guesses only; in general they agree with those of other workers, e.g. Jackson & Rawlings (1997).

constant reflecting the geometry of the beamed component – $m = 2$ will be used for jets.

As discussed above, relativistic beaming is often used as an explanation for the observed one-sidedness of jets, and for the greater prominence of jets and cores in quasars as compared to NLRG. Measurements of superluminal motion in the parsec-scale jets of quasars and BLRG (corresponding to the cores seen on maps of the large-scale radio structure) have established that relativistic velocities are present there. In analysing the present sample we shall compare the properties of features which might be supposed to be beamed, with the aim of establishing the degree to which relativistic velocities persist on large scales.

1.3 Definitions and conventions

In what follows we shall make extensive use of terms describing the features of radio sources, and so some definitions are important. We use the traditional term ‘core’ for the component, normally unresolved on arcsecond scales and having a flat spectrum, which coincides with the central regions of the optical host galaxy. B94 use the term ‘central feature’ for these components. A ‘jet’ is a feature conforming to the definition of Bridle & Perley (1984); it is at least four times as long as it is wide, separable at high resolution from other extended structure, and aligned with the core where it is closest to it. ‘Possible jets’ are features that are not four times as long as they are wide (they may be knots or trains of knots), or that have not been imaged at high resolution, but which meet the other criteria for a jet and are plausible tracers of the ‘beam’, the underlying stream of particles. We generally use the term ‘jet’ for the brighter jet in the source (or the only jet if only one is detected) and the term ‘counterjet’ for the fainter jet where one is present. ‘Hot spots’ are structures associated with the termination of the beam. We follow the definition of L97 and H97, who define them as features that are not part of a jet and that have a largest dimension smaller than ten per cent of the main axis of the source, a peak brightness greater than ten times the r.m.s. noise, and a separation from nearby peaks by a minimum falling to two thirds or less of the brightness of the fainter peak. In this paper we shall be interested in the most compact or ‘primary’ hot spots, which seem likely to be the regions where the beam terminates.

Values of $H_0 = 50 \text{ km s}^{-1} \text{ Mpc}^{-1}$, $q_0 = 0$ are used throughout this paper.

2 ANALYSIS AND RESULTS

2.1 The sample

The source information for the combined sample is shown in Table 1.

B92 selected 3CR sources with $P_{178} > 1.5 \times 10^{25} \text{ W Hz}^{-1} \text{ sr}^{-1}$ and $z < 0.15$. They excluded sources known not to have hot spots (wide-angle tail, fat-double and cluster-centre objects) and three giant radio galaxies. In addition, they did not image the sources included by LRL from outside the 3CR catalogue; DA 240 and 4C 73.08 would have met their selection criteria but could be excluded as giants in any case. Conversely, almost all the sources selected by B92

but not LRL are only excluded from LRL's sample on the grounds of position on the sky [the exceptions are 3C 197.1, 3C 223.1 and 3C 277.3 which have $S_{178} < 10.9$ Jy on the Baars et al. (1977) scale]. All the sources in the LRL-based sample defined in H97 meet the power criterion used by B92, and sources from 3CR are only excluded on the basis of position on the sky or $S_{178} < 10.9$ Jy. Thus, although the combined sample is not strictly flux-complete, we do not believe it to be biased in any way which should affect our analysis, and a complete sub-sample consisting of the non-giant LRL sources (34 in total) can be constructed if completeness is an issue; the objects drawn from this sample are marked in bold type in Table 1. Possibly more serious than the power and flux density constraints from the point of view of bias is the exclusion from our LRL-based sample of sources classed by them as FRIs. This excludes some objects which are in other respects similar to those in our sample; for example, 3C 288 (Bridle et al. 1989) and 3C 346 (Spencer et al. 1991) are excluded, though they are very similar in appearance to 3C 438 or 3C 15. Generally this bias manifests itself as an exclusion of sources that have structure intermediate between classical FRIs and FRIIs, and so does not affect conclusions based on the sample of sources with classical FRII structure (the most obvious indicator of this being well-defined hot spots).

178-MHz flux densities were taken from LRL where possible, and otherwise determined following the prescription in LRL, correcting to the scale of Baars et al. (1977). The 178-MHz flux densities and low-frequency spectral indices of the sources in the sample of B92 are discussed in L97.

The sample of quasars observed by B94, which we use for comparison with our results, consists of 13 quasars from LRL with angular sizes greater than 10 arcsec. The redshifts of these objects range from 0.311 to 2.012, with the median redshift being 0.77. Because of the selection criteria, the sample is biased towards larger linear sizes with respect to LRL quasars as a whole. The biasing and the inclusion of sources at very much larger redshifts and luminosities than those of our sample mean that the B94 sample is not ideal for such comparisons; however, it is the only sample for which information on quasar jets is presently available.

2.2 Analysis of radio maps

High-resolution, well-sampled electronic radio maps were available to us for 44 of the 50 sources. The remaining six objects were omitted essentially randomly, and so do not bias the discussion. From these images we have measured various parameters which relate to energy transport in these sources. These are discussed below.

With the exceptions noted in individual tables, the flux densities given are taken from VLA maps, and are therefore subject to errors of a few per cent because of the limiting accuracy of the absolute calibration of the VLA. This error has not been included in the errors quoted.

For ease of tabulation, we have divided the jets, lobes and hot spots of each source into 'north' and 'south'.

2.2.1 Total and lobe flux densities

A reliable measurement of the total flux density of a source could be obtained from direct integration on low-resolution

maps only if the object had been observed with sufficient short-baseline coverage to sample all the large-scale structure. This was true of most objects observed in H97, but a number of the objects from the sample of B92 were undersampled due to insufficient observation or large angular size. In these cases (see Table 2) integrated flux densities are taken from the literature or estimated by interpolation of the integrated spectrum. Reliable flux densities of individual lobes are generally only available for the well-sampled sources (Table 3), though in some cases a zero-spacing flux density from the literature was used to constrain the short baselines in maximum-entropy mapping routines. It was sometimes difficult to separate the emission from the two lobes; this is indicated by a correspondingly large error in Table 3. Largest angular sizes of the sources were measured directly from the maps, and the distance from the core to the most distant region of lobe emission is also tabulated so as to define a measure of hot spot recession comparable with that of B94 – in the few 'winged' sources where the greatest distance or the largest angular size was in a direction transverse to the source axis, this is noted and an alternative distance given.

2.2.2 Cores

In general the radio cores of the objects in the sample were unresolved with the highest resolution of the VLA. The cores were therefore well fitted by an elliptical Gaussian plus baseline (using the AIPS task JMFIT). The integrated flux densities determined by these fits are given in Table 2; errors are the formal 1σ errors from the fitting routine.

2.2.3 Jets and counterjets

It is possible, as discussed in B94, to measure the flux density of jets in a number of different ways. Clearly a simple measurement of the flux density of the jet region (as in B92) is not useful, even if the jet region is well defined, because of the necessity of correcting for background emission (particularly important in these objects where the jets have low contrast with the lobes). In addition, in a number of cases the jet region is not well defined, particularly where the jet is entering a hot spot.

To allow a comparison with the results of B94, we determine jet flux density using their methods. The total jet flux density is obtained by integrating over the area that clearly contains jet emission, correcting for the background by integrating a similarly-shaped area on either side and subtracting the average of these measurements normalised to the area of the jet integration. We repeated this process three times for each jet and for counterjets where present. Errors are assigned by considering the standard deviation of the integrated and the normalising values, and combining the resulting errors in quadrature. Where there is a substantial difference between the background flux densities on the two sides of the jet, this will dominate the error assigned.

Where even the most tentative jet or counterjet candidate is detected, we have chosen to record its flux density. (Flux densities of 'possible' jets are marked with an asterisk in Tables 4 and 5.) Where there was no detection of any sort, we have tried to determine an upper limit on the flux

density of a present but undetected jet. There is no way in which a truly conservative upper limit can be set on flux density from an unseen jet, given the number of possible forms that jets can take, but some reasonable approximations can be made to a plausible limit that most unseen jets will not exceed. For compatibility with the measurements of B94 we defined total jet limits in a similar way. On maps of intermediate resolution we integrated over the rectangle two beamwidths wide between the core and the primary hot spot (chosen as the most plausible path for a jet) or the closest approach which did not intersect bright confusing lobe emission, and over the two rectangles on either side of it. If the flux density in the central rectangle was larger than that in the other two, we subtracted the mean flux density of the edge rectangles from that of the central one and used the result as an upper limit. Otherwise, we used the positive difference between the central flux density and the lower of the two edge flux densities as the upper limit. This way of assessing the upper limits has the advantages that the number obtained increases with the inhomogeneity of the lobe (the correct behaviour, since jets are hidden by confusing lobe structure as much as by on-source noise), and that when measured on a lobe that *does* have a jet the upper limit is a reasonable measure of the jet's true flux density. The obvious disadvantage of this method is that it is resolution- and sensitivity-dependent, and that a subjective decision must be taken to make the measurements from a particular map; where only low-resolution maps were available to us, the limits are higher.

We also measured straight jet flux density. As B94 point out, FRII radio sources often have a relatively straight inner section followed by a bent region. Regions of bending are likely to be the sites of strong interaction between the jet and its environment, which introduces a further source of random scatter into the measurements; it is also impossible to apply a simple relativistic beaming analysis (section 1.2) to a bent jet, since there is not a single value of the angle made by the beam to the line of sight. The straight jet region is defined, following B94, to be a rectangle, aligned with the core, over which the line of the brighter or only jet deviates from the centerline of the rectangle by less than a jet radius and which avoids any significant confusion with lobe emission. (Thus, when the jet enters a hot spot or region of high surface brightness, the straight jet is considered to end.) The rectangle was taken from the core to the furthest extent of the straight jet, even where the straight jet was only visible in part of the lobe, to maximise the chances of a counterjet detection. Identically-sized rectangles on either side of the straight jet region were integrated to provide an estimate of the background flux density. The similar rectangular region on the other side of the core was integrated to provide an estimate of the flux density from the counterjet, if present, or an estimated limit on its flux density if not (if the central value was higher than the values on either side, their average was subtracted; if not, the positive difference between the lower value and the central value was used as an upper limit). As before, three measurements were made on each source and averages taken; errors were assigned in the same way as for the total jet flux densities. The straight jet fluxes are tabulated in Table 5. Most of the objects with well-defined counterjets have an angle of not quite 180° between jet and counterjet; counterjet measurements of this

sort can thus underestimate the counterjet flux density. On the other hand, the counterjet rectangle can intersect confusing emission in the counterjet lobe, and therefore seriously overestimate the counterjet flux density. These results should therefore be treated with some caution. Where there was no candidate straight jet in either lobe, no entry is made in Table 5. In these cases the upper limits on total jet flux, discussed above, may be taken as upper limits on straight jet flux.

All the errors on the jet flux density determinations are conservative, because of the difficulty in deciding which parts of the object should be treated as a jet or counterjet. In a few cases interpretation is crucial; these are now discussed.

- 3C 192: we have only considered the jet seen near the S hot spot complex in the high resolution maps of L97. The inclusion of the faint linear feature seen in the S lobe at low resolution – which is not clearly aligned either with the core or with the hot spots – would increase the jet flux density substantially.
- 3C 234: we have only considered the jet leading into the northern hot spot. If the ridge E1 of H97 were included (as it is in the straight jet flux density determination) the integrated jet flux density would be substantially higher.
- 3C 300: It is not clear how much of this object's north lobe should be classed as a jet. We omitted the last few arcseconds where there is no surrounding lobe emission. The flux density might be increased by up to 15 mJy if this region were included.
- 3C 327: we have differed from L97 in counting the faint linear features in both lobes as possible jets. If only the jet candidate around the core is considered, the flux density is approximately 0.4 mJy.
- 3C 390.3: we only consider material closer to the core than knot B of Leahy & Perley (1995), on the grounds that knot B is the primary hot spot.
- 3C 403: we only consider the regions F7, F8 of B92 as true jet, on the grounds that F6 is the primary hot spot. Including F6 and the jet-like components F4 and F5 would increase the flux density to 80 mJy.
- 3C 424: we have not considered the northern 'jet' of this object to be a true jet. It is however quite possible that some of the internal structure in this northern component should be treated as jet material. We have treated S3 as the only jet component in the southern lobe. The reasons for this treatment are discussed in L97.

2.2.4 Hot spots

As in H97, we attempt to identify a 'primary' hot spot in each lobe. Flux and size measurements are tabulated for the primary components only. Cases where the identification of the primary hot spot might be ambiguous are discussed in the notes to Table 6.

B94 measure the flux densities and dimensions of the hot spots in their quasar sample by fitting with a Gaussian and baseline. They remark that such models do not always represent the hot spots well, and the situation is still more difficult in the present sample with its considerably higher spatial resolution and with a more relaxed definition of the term 'hot spot'. The procedure we have adopted is as follows, therefore: we have tried to fit models consisting of a

Gaussian and baseline to all but the most obviously resolved hot spots, running the fitting routine a number of different times on slightly different regions or with slightly different initial guesses. Where these different fits gave essentially the same results, we have tabulated in Table 6 the average values of the integrated flux densities and major and minor axis lengths; the error on the flux densities is estimated from the range of the results of different measurements. Where the fits were obviously poor, and diverged significantly (by a factor of 1.5 or more in flux density either way) on small alterations of the initial parameters of the fitting routine, we measured the sizes of the components by taking slices through them and estimating the FWHM, or in extremely resolved cases by simple measurement from maps; we measured the flux densities by integration from the maps, with a rough correction for background emission from integration over a nearby part of the lobe. The errors in the derived hot spot flux densities in these cases are an estimate of the error from direct integration, taking into account the difficulty of deciding exactly which was the hot spot region.

The distances of the hot spots from the cores are also tabulated.

3 TRENDS

The high-frequency flux densities we use in this section have all been corrected to an observing frequency of 8.4 GHz for ease of comparison. Cores are assumed to have flat spectra ($\alpha = 0$) and jets to have $\alpha = 0.8$. Total flux densities are scaled using the low-frequency (178–750 MHz) spectral index, which is available for the whole sample. Errors in these corrections should not badly affect the results of the analysis performed here.

Uniform symbols are used in the plots in this section. Open circles represent LERG, open triangles indicate NLRG, filled triangles indicate BLRG and filled stars indicate quasars. The one unclassified object, 3C 136.1, is plotted as a dotted circle and is not included with any class of object where the objects are separated by emission-line type.

The ‘prominence’ of a feature is defined throughout as the ratio of the flux density of a given feature to the extended flux of the source (i.e. the total flux density of the source minus contributions from jets and cores). This is a useful quantity for indicating effects due to relativistic beaming, since the extended flux density of the source should be orientation-independent.

The median values of some of the distributions discussed below are tabulated, broken down by object class, in Table 7. For comparison, the median values using only objects drawn from the complete sample of LRL are also tabulated. It will be seen that in general the addition of the non-LRL objects makes little difference to the distributions. All the results that follow are based on the full sample.

3.1 Large-scale structure

Fig. 1 shows the power-linear-size diagram for the whole sample. The sources populate a range of two decades in luminosity, if the brightest objects (Cygnus A, 3C 123 and 3C 438) are not counted, and approximately 1.5 decades in

linear size (the upper limit in this plot is due to the exclusion of the giants; the lower limit is due to the absence of compact sources from LRL at low redshifts).

It will be seen that there is a tendency for the LERG to be smaller; the distribution of linear sizes of these objects is strongly peaked around the 100-kpc range, with a median of 130 kpc compared to 370 kpc in the sample as a whole. A Wilcoxon-Mann-Whitney test rejects the hypothesis that the LERG in this sample are drawn from a size distribution with the same median as that of the other objects at the 99.9 per cent level; even if the giant radio galaxies (some of which are LERG) are included in the test, the samples are still significantly different. We shall return to this initially surprising fact, first noted by Black (1992) for his sub-sample of these objects, in a further paper. The median linear size of BLRG objects is smaller than that of NLRG but the difference between the two distributions is not significant. In the larger and higher-power sample of L94 the broad-line objects are significantly smaller.

The median linear size of the B94 quasars is comparable to that of the radio galaxies (Table 7). However, the B94 sample is biased towards larger linear sizes because of the angular size selection criterion, so this comparison is probably not very meaningful.

3.2 Hot spots

There is a strong positive correlation (significant at the 99.9 per cent level on a Spearman Rank test), with slope approximately unity, between linear size and hot spot size in the 43 sources in the sample with measured hot spots (Fig. 2). Hot spot size is defined here as the average of the sizes of the two hot spots at either end; the size of an individual hot spot is defined as the geometric mean of the largest and smallest angular sizes. Care must be taken when comparing the sizes of hot spots in different objects, since they have been measured from maps of differing angular resolution; objects of large angular size are more likely to have been mapped at lower resolution in this sample. However, the correlation is also present when only those measurements made from maps of ~ 0.23 arcsec resolution are considered, suggesting that an intrinsic correlation exists. This result provides some support for suggestions in Laing (1989) and B94 that the hot spot sizes scale with source linear size; however, Black (1992) found no such correlation in the sub-sample of these objects that he analysed. If the correlation is real, it is consistent with self-similar models for these sources (e.g. Kaiser & Alexander 1997) or may be evidence for ‘tired jet’ models in which the jet decelerates with distance from the core (B94). It is evidence against models in which the beam size is independent of the linear size of the source (e.g. magnetic self-confinement).

Comparing the sizes of hot spots within a single source does not suffer from these difficulties. Of the 32 sources with detected jets or possible jets and measurements of hot spot size, 24 had hot spots that differed in area by more than 25 per cent. Of these 15 (62 per cent) had the brighter or only jet pointing towards the more compact hot spot. This lack of a significant trend contrasts with the results of B94 who found that, where the hot spots were significantly different in size, the jets in their sample of quasars always pointed towards the more compact hot spots. They found a depen-

dence of hot spot size ratio on core power which is absent in this sample. B94 also found a trend for the hot spot on the jetted side to be more recessed (where recession is measured by the ratio of the core-hot spot distance to the lobe length) whereas in the present sample the jetted hot spot was *less* recessed in 21 (65 per cent) of the 32 sources, a marginally significant trend (significant at the 90 per cent level on a binomial test).

22 sources with jets in the present sample had one hot spot brighter than the other within the errors assigned. The brighter or only jet pointed towards the dimmer hot spot in 7 cases and towards the brighter in 15 (68 per cent) – a marginally significant trend (significant at the 90 per cent level on a binomial test). This may be contrasted with the results of Laing (1989), who found that 26/30 sources with jets had the jet pointing towards the brighter hot spot in a sample of powerful radio galaxies and quasars. It would appear that all the results relating to hot spots are weaker, if present at all, in this sample than in high-redshift samples containing quasars. This is understandable if the trends in the B94 sample are due to relativistic effects (as suggested by theory; e.g. Komissarov & Falle 1996), since at least some of the objects studied here cannot be strongly beamed towards us.

Best et al. (1995) have analysed the hot spot separation ratios of a large sample of FRII radio sources (with some overlap with the present sample, but including many high-power sources), showing that there are significant differences between the distributions of radio galaxies and quasars. The quasars are more asymmetrical, a fact that they attribute to mildly relativistic hot spot advance speeds. They concluded that in the low-redshift régime there was no difference between the hot spot separation ratios of BLRG and NLRG, but were unable to test whether the LERG formed a distinct population. In Fig. 3 we show histograms of the fractional separation difference x [$x = (\theta_1 - \theta_2)/(\theta_1 + \theta_2)$, where θ_1 and θ_2 are the lengths of the longer and shorter lobe respectively] for the 40 objects in this sample with measured hot spot positions. It will be seen that the distributions are not markedly different for the NLRG and the LERG, and a Wilcoxon-Mann-Whitney test finds no significant probability that the two are drawn from different distributions. The broad-line objects appear *more* symmetrical than the narrow-line objects (a result significant at the 97 per cent level on a Wilcoxon-Mann-Whitney test). These results are both rather surprising; in the simple models outlined above we would expect BLRG to be more asymmetrical than the NLRG, because of their smaller mean angle to the line of sight, while LERG should also be more asymmetrical than NLRG if they are an isotropically distributed population. This may be evidence that in this comparatively low-redshift and low-power régime environmental effects on source symmetry are dominant over light travel time effects.

3.3 Jets

In the sample as a whole 29/50 (58 per cent) of objects have definite jet detections and 40/50 (80 per cent) have possible or definite jets. The jet detection rates are not significantly different in the two sub-samples of B92 and H97. There appears to be no dependence of jet detectability on luminosity over the luminosity range studied here; this is

shown in Fig. 4, a plot of jet prominence against luminosity for the 44 sources with measured jets or possible jets or upper limits together with the B94 quasars. In all but two cases radio galaxy jets have less than 6 per cent of the extended flux density of the source, and the typical value is nearer to 1 per cent. Parma et al. (1987) found an inverse correlation between jet prominence and luminosity in a sample of lower-power (mostly FRI) objects, but we find no such strong relationship in FRIIs over our luminosity range. Where the luminosity ranges overlap our results are consistent with those of Parma et al., so it seems likely that their results are indicative of an increase in jet efficiency across the FRI/FRII boundary which has levelled out by the luminosity range of our sample.

Jets are one-sided. In the sample as a whole 16 objects (32 per cent) have possible counterjet detections, but only 6 (12 per cent) have definite detections, these being the unusual objects 3C 15, 3C 171 and 3C 438, the bright, deeply imaged objects 3C 405 and 3C 353, and the highly symmetrical source 3C 452. The counterjet candidate detection fraction is thus below that of B94 in their sample of quasars (54 per cent have counterjet candidates), which is a surprising result in the context of unified models.

In the only independent search for jets recently conducted, Fernini et al. (1993) imaged a sub-sample of five objects with powers matched to those of the B94 quasars, and found only one definite jet (but three possible jets). Although the sensitivity in this study should have been comparable to that of our observations, the spatial resolution was lower by a factor of 2 because of the higher redshift of these objects and the lower angular resolution of the observations. Too much should not be read into the differing jet detection fractions, as the sample is small.

Perhaps surprisingly, the jet detection fraction is not very different in the different classes of object studied here. Of the 15 low-excitation objects, 9 (56 per cent) have definite jets and 11 (73 per cent) have possible or definite jets. For the 9 BLRG, the figures are 7 (78 per cent) with definite jets and the same number with definite or possible. The 25 NLRG have 13 definite jets (52 per cent) and 22 definite or possible (88 per cent). None of these jet detection fractions are sufficiently different to provide evidence that the different classes of object are drawn from different populations. L94 found a much more marked difference between the jet detection fractions of broad-line objects (including quasars) and NLRG in their higher-power sample.

It is perhaps unexpected, in the model in which the BLRG are quasar counterparts, that there should be two (3C 227 and 3C 381[†]) with no indication of a jet – compare the universal jet detection in the B94 quasars. On the other hand, several of the BLRG that do have jets are very similar in appearance to the quasars. The median straight jet prominence of the BLRG is twice that of the NLRG (Table 7) and the difference between the samples is significant at the 95 per cent level on a median test (the only simple test that can be applied rigorously, given the number of upper limits in the data).

Fig. 4 shows that the distribution of BLRG total jet prominence overlaps with the low end of quasar total jet

[†] The classification of 3C 381 as a BLRG is uncertain; see H97.

prominence; the B94 quasars include objects with total jet prominence much higher than in either the BLRG or the NLRG, and this is reflected in the higher median total jet prominence of the quasars (Table 7); the difference between BLRG and quasars is significant at the 95 per cent level on a median test. However, the prominences of *straight* jets in the BLRG and the B94 quasars are similar; the distributions cannot be distinguished on a median test.

Black (1992) noted a tendency for jets to be detected in shorter objects. In the present sample 24 of the 40 radio galaxies with definite or possible jets (60 per cent), have linear sizes less than the median size for the whole sample of 370 kpc, a trend significant at the 90 per cent level. These results are weaker than those of Black (1992), probably because of the detection or possible detection of a number of faint jets in larger sources since his analysis. Fig. 5 shows that the weak trend for jet prominence to be related to length is entirely because of the existence of a number of short, low-excitation objects with prominent jets; 3C 15 and 3C 401 are examples of this class, which overlaps in its radio properties with the ‘jetted double’ class of Law-Green et al. (1995), as discussed by H97.

There is no significant tendency for the brighter or only jet to lie in the longer lobe (18/33) or the brighter lobe (16/26). Such trends might be expected if relativistic and light-travel-time effects dominated the appearance of radio sources.

The lengths of the jets and straight jets are strongly correlated (> 99 per cent significant on a Spearman Rank test) with the total length of the source. This is also consistent with self-similar models for the sources, and militates against models which define a scale length for the jet or the onset of jet bending (e.g. any model which relates these quantities to galactic scale sizes). There is no significant correlation between straight jet flux density and length, however.

3.4 Jet sidedness

The jet-counterjet ratio should be an indicator of the velocities involved and the projection angles in models based on relativistic beaming. If the jet and counterjet are intrinsically symmetrical, then their relative flux densities are found from equation (1). For the reasons given in section 2.2.3, the straight segments of jets are best for this kind of test. In general the ratio J , the straight jet sidedness, is given by

$$J = R \left(\frac{1 + \beta_j \cos \theta}{1 - \beta_j \cos \theta} \right)^{2+\alpha_j} \quad (2)$$

where R is the degree of *intrinsic* asymmetry (the ratio between the rest brightnesses of jet and counterjet) and might represent the effects of different environments on the efficiencies of the two beams (neglecting the effects such environments might have on velocities). It follows from equation (2) that, if relativistic beaming effects are dominant in the jets, objects at smaller angles to the line of sight should have larger jet-counterjet asymmetries.

Fig. 6 shows the distribution of straight jet sidednesses for the radio galaxies with detected jets and for the B94 quasars. Dashed areas of the histograms represent *lower* limits on the jet-counterjet ratios (since they are calculated

using upper limits on the counterjet flux density). Clearly selecting on detected jets biases the sample; in the context of unified models, sources without detected jets will be preferentially unbeamed and so the more two-sided sources are excluded from the plot.

The plot as it stands can at best be said to be consistent with unified models (which would not be the case if, for example, the radio galaxies were obviously more one-sided than the quasars). However, the paucity of counterjet detections in the radio galaxy population is surprising if unified models are correct (though the counterjet detection fraction is underestimated by this plot which excludes non-aligned counterjets in, for example, 3C 15 and 3C 438).

3.5 Cores

The prominence of the radio core is commonly used as an orientation indicator in studies of beaming in radio galaxies and quasars (e.g. Orr & Browne 1982). Various authors (e.g. Kapahi & Murphy 1990; L94; Morganti et al. 1995; Morganti et al. 1997) have attempted to show consistency between the distribution of core prominences and the predictions of unified models.

In the present sample, the median core prominence of BLRG is nearly an order of magnitude greater than that of the NLRG (Table 7) and a Wilcoxon-Mann-Whitney test allows us to reject the hypothesis that the core prominences for the two classes are drawn from a distribution with the same median at > 99 per cent confidence. Morganti et al. (1997) find a similar difference between the median core prominences of BLRG and NLRG. The core prominences for both broad-line and narrow-line objects have a scatter of 2–2.5 orders of magnitude.

The LERG have a median intermediate between the broad- and narrow-line objects (as they do in L94 and in the largely disjoint sample of Morganti et al. 1997) and a Wilcoxon-Mann-Whitney test does not distinguish the median core prominence of the LERG from that of the high-excitation objects with significant probability. In the simple versions of unified models discussed above (section 1.1) we might expect the core prominences of LERG to be distributed like those of the broad- and narrow-line objects combined, which does not seem to be the case in this sample (there is a lack of low-excitation objects with very bright cores). This result is only marginally significant (at the 90 per cent level on a Kolmogorov-Smirnov test).

The core prominences of BLRG and B94 quasars are similar; the medians are very close (Table 7) and the distributions are not distinguished by a Wilcoxon-Mann-Whitney test. This result differs from that of Morganti et al. (1997) who found a significant difference between the core prominences of FRII quasars and BLRG. We discuss this further in section 4.2.

There is no apparent trend in the core prominences as a function of luminosity. However, on a plot of core prominence against linear size (Fig. 7) the NLRG (only) show an apparent positive trend (significant at > 99 per cent on a Spearman Rank test); i.e. for NLRG, a longer source tends to have a more prominent core. There is no tendency for the extended flux densities in these objects to anticorrelate with length, so this trend, though surprising, must be real.

If we believe that the core is a beamed parsec-scale

jet (as suggested by VLBI observations) and that the one-sidedness of jets is a relativistic effect, there should in principle [equation (1)] be a relationship between the prominence of jet and core, assuming that the beam does not change direction significantly between parsec and kiloparsec scales. In general, the velocity in the core may not be equal to that in the kiloparsec-scale jet, and so the slope of a jet-core prominence relation will not be unity. B94 investigate the relation between core and jet prominence for their sample of quasars, and conclude that there is such a relationship, with deceleration required between the parsec- and kiloparsec-scales. Fig. 8 shows a plot of total jet prominence against core prominence for the present sample.

B94 chose to investigate the relationship between the core and *straight* jet prominence. They point out that a well-defined relationship between the core and jet beaming factors only occurs when the two are at the same angle to the line of sight. As soon as the jet is seen to bend, the emission is beamed differently and the simple relationship is lost. This could be used to explain the absence of a strong relationship in Fig. 8.

In Fig. 9 we plot the relationships between (brighter) straight jet and core prominences for the well-mapped sources in the present sample and for the quasars of B94. Unlike them, we have made no attempt to assign some of the flux density from the core to the straight jet, as we have little information on the VLBI properties of the radio galaxies. This weakens the correlation observed by B94 for their sample, though it is still significant at the 90 per cent level on a Spearman Rank test. Because the cores and straight jets of the BLRG and of the quasars are more prominent than those of the NLRG, as discussed above, there is a weak but significant positive trend in Fig. 9, even in the presence of upper limits [> 95 per cent on a generalised Spearman Rank test, as implemented in the survival analysis software package ASURV Rev. 1.1 (LaValley, Isobe & Feigelson 1992)]. This is true whether or not the B94 quasars are included in the correlation analysis.

Also noticeable in Fig. 9 is a population of LERG whose straight jets are much brighter than those of other objects of similar core prominence.

4 DISCUSSION

We summarise the important results of section 3 in Table 8. In this section of the paper, we discuss some interesting general properties of the sources that have emerged from our analysis, examine the evidence for unification in this sample, and consider ways in which the data can be modelled.

4.1 General radio galaxy properties

Jets or possible jets are detected in most of the sources in the sample, and we have been able to measure, or put upper limits on, the background-subtracted flux densities of the jets of the objects in the sample for which we have good maps. There is no strong dependence of the prominences of these jets either on the luminosity of the radio galaxy or on its linear size. These results make it seem likely that with even better observations we should be able to detect jets

in all FRII radio galaxies. Further observations of higher-luminosity radio galaxies, which are more directly comparable to quasars, are necessary to investigate these results further.

Core prominence shows no trend with luminosity in the present sample (but cf. the anticorrelation seen in the larger samples, spanning a wider luminosity range, of Giovannini et al. 1988 and Zirbel & Baum 1995). In the NLRG alone, core prominence is positively correlated with source length (the BLRG and quasars and the LERG show no significant correlation). Source length is affected by angle to the line of sight, but the dominant contribution to the distribution of source lengths must be intrinsic (in any case, a simple beaming model with constant-length sources would predict an *anti-correlation* between source linear size and core prominence). The normalising extended flux density is not correlated with linear size. It appears therefore that there is a direct relation between core prominence and total source length, at least in the NLRG; relativistic beaming and projection effects might be expected to wash out such an effect in the BLRG and quasars. The physics behind such a correlation is unclear, but it will be interesting to see whether it persists in larger samples.

Both the linear sizes of the hot spots and the lengths of the straight jets are strongly, and approximately linearly, correlated with the total linear sizes of the radio source. This seems to rule out models which set scale sizes on either the width of the beam or the distance it can travel without disrupting.

4.2 Unified models and relativistic velocities

In section 1.1 we pointed out that the absence of lobe-dominated quasars from our sample *requires* that some of these radio galaxies be oriented at small angles to the line of sight. We outlined a model in which some or all of the BLRG in the sample are the low-redshift counterparts of quasars.

We have seen that the BLRG have systematically brighter cores and straight jets than the NLRG, and that the distributions of these quantities and of jet sidedness in the BLRG are very similar to those of the B94 quasars (although, as pointed out above, those objects are not an ideal population for the comparison). These results are consistent with a model in which the cores and jets in BLRG are preferentially beamed [as expected in most unified models and concluded, in the case of cores, by Morganti et al. (1997)] and in which the BLRG are similar in their orientations to quasars.

There remain a number of problems with simply identifying all broad-line radio galaxies as low-power lobe-dominated quasars. The facts that some BLRG in our sample have no detected jets, and that the BLRG appear more symmetrical than the NLRG, may perhaps be attributed to random environmental effects, given the size of the sample, or to misclassification. The fact that the *total* jet prominences of the B94 quasars are very much higher than those of our BLRG is interesting; there appear to be no BLRG in our sample comparable to the jet-dominated objects in the B94 sample (e.g. 3C9). Since these results imply that the quasar jets are significantly brighter after they bend, it is hard to explain it as a simple relativistic beaming effect;

it may indicate real differences in jet efficiency, power or environment between the low-redshift BLRG and the high-redshift quasars.

As discussed above, Morganti et al. (1997) found that BLRG cores in their sample were systematically less prominent than those of lobe-dominated quasars, even after selection effects were taken into account. However, as they point out, the redshift distributions for the BLRG and quasars in their sample are very different, and their sample, like ours, contains, at $z \lesssim 0.3$, very few lobe-dominated quasars and many BLRG. At high redshifts BLRG and quasars are known to coexist, and our results are not inconsistent with the suggestions of Barthel (1989) and Morganti et al. (1997) that high- z BLRG are transitional objects.

When the prominences of straight jets and cores are compared (Fig. 9), a weak positive trend can be seen in the sense that objects with more prominent cores tend to have more prominent jets. This trend is unlikely to be much affected by the fact that some of the points are upper limits. The trend is in agreement with the results of B94, and the slope of the correlation is certainly less than unity. Such a result is expected if, as suggested by B94, both the cores and jets are beamed, with the emitting material in the jets having an effective bulk velocity lower than that seen in the core. Given that we expect the cores to be beamed for other reasons, it is hard to explain such a correlation without relativistic velocities in the radio galaxy jets as well. The sidednesses of the jets, when compared to those of the jets in B94, are also consistent with such a model, although the result is weak since there are few good counterjet detections.

Our results on the core prominence of LERGs are broadly consistent with the suggestion that they form an isotropic population, as found by L94. However, there is (in this sample) a paucity of LERG with very bright cores, and there is also a sub-class of these objects with very prominent jets and diffuse, weak hot spots; the LERG are also significantly smaller than the high-excitation objects. These results suggest that there is some physical difference, either intrinsic or environmental, between the radio properties of the LERG and the other objects; we shall explore the reasons for this difference elsewhere.

We find no relationship between the jet side and the more compact or the brighter hot spot; this is consistent with the suggestion that these effects, seen by B94 and L89, are due to relativistic beaming in the hot spot and that the present sample is less beamed than those previously investigated because of a wider range of angles to the line of sight.

4.3 Modelling: future work

These results allow us to fit empirical models to the jet and core prominence data and the jet sidedness data, with the input being the distribution of angles to the line of sight and the intrinsic length distribution of sources; the ability to ignore the luminosity distribution and its relation to linear size is an important simplification. Free parameters to a model fit would include the bulk velocities in jets and cores, a parametrisation of the dependences of the prominences of both on linear size, and some normalising ‘intrinsic prominence’, corresponding to the unbeamed prominence of the jet and core; in addition, some parametrisation of the distribution both of velocities and of intrinsic prominences (which

might depend on source environment) might be necessary. Such model fitting has been done before on projections of datasets of this type (e.g. Morganti et al. 1995; Wardle & Aaron 1997) but we are in a position to use the relationships between the measured quantities, and so to put tighter constraints on the allowed regions of parameter space. We shall discuss results of this type of analysis in a further paper.

ACKNOWLEDGEMENTS

MJH acknowledges a research studentship from the UK Particle Physics and Astronomy Research Council (PPARC) and support from PPARC grant GR/K98582. We are grateful to Alan Bridle, Jack Burns, David Clarke, Jane Dennett-Thorpe, Paddy Leahy, Mark Swain and Wil van Breugel for supplying images used in the analysis, and thank Peter Scheuer and Christian Kaiser for useful discussions. We thank an anonymous referee for a number of helpful suggestions which allowed us to improve the clarity of the paper.

The National Radio Astronomy Observatory is operated by Associated Universities Inc., under co-operative agreement with the National Science Foundation. This project made use of STARLINK facilities. This research has made use of the NASA/IPAC Extragalactic Database (NED) which is operated by the Jet Propulsion Laboratory, California Institute of Technology, under contract with the National Aeronautics and Space Administration.

REFERENCES

Alexander P., 1985, PhD thesis, University of Cambridge
 Baars J.W.M., Genzel R., Pauliny-Toth I.I.K., Witzel A., 1977, *A&A*, 61, 99
 Barthel P.D., 1987, in Zensus J., Pearson T., eds, *Superluminal Radio Sources*, Cambridge University Press, Cambridge, p. 148
 Barthel P.D., 1989, *ApJ*, 336, 606
 Barthel P.D., 1994, in Bicknell G.V., Dopita M.A., Quinn P.J., eds, *The First Stromlo Symposium: the Physics of Active Galaxies*, ASP Conference Series vol. 54, San Francisco, p. 175
 Best P.N., Bailer D.M., Longair M.S., Riley J.M., 1995, *MNRAS*, 275, 1171
 Black A.R.S., 1992, PhD thesis, University of Cambridge
 Black A.R.S., Baum S.A., Leahy J.P., Perley R.A., Riley J.M., Scheuer P.A.G., 1992, *MNRAS*, 256, 186 [B92]
 Bridle A.H., Fomalont E.B., Byrd G.G., Valtonen M.J., 1989, *AJ*, 97, 674
 Bridle A.H., Hough D.H., Lonsdale C.J., Burns J.O., Laing R.A., 1994, *AJ*, 108, 766 [B94]
 Clarke D.A., Bridle A.H., Burns J.O., Perley R.A., Norman M.L., 1992, *ApJ*, 385, 173
 Cohen R.D., Osterbrock D.E., 1981, *ApJ*, 243, 81
 Dennett-Thorpe J., 1996, PhD thesis, University of Cambridge
 Eracleous M., Halpern J.P., 1994, *ApJS*, 90, 1
 Fanaroff B.L., Riley J.M., 1974, *MNRAS*, 167, 31P
 Fernini I., Burns J.O., Bridle A.H., Perley R.A., 1993, *AJ*, 105, 1690
 Giovannini G., Feretti L., Gregorini L., Parma P., 1988, *A&A*, 199, 73
 Hardcastle M.J., Alexander P., Pooley G.G., Riley J.M., 1997, *MNRAS*, 288, 859 [H97]
 Hine R.G., Longair M.S., 1979, *MNRAS*, 188, 111
 Jackson N., Rawlings S., 1997, *MNRAS*, 286, 241

Kaiser C.R., Alexander P., 1997, MNRAS, 286, 215

Kapahi V.K., Murphy D.W., 1990, in Zensus J.A., Pearson T.J., eds, *Parsec-scale Radio Jets*, Cambridge University Press, Cambridge, p. 313

Komissarov S.S., Falle S.A.E.G., 1996, in Hardee P.E., Bridle A.H., Zensus J.A., eds, *Energy Transport in Radio Galaxies and Quasars*, ASP Conference Series vol. 100, San Francisco, p. 327

Laing R.A., 1989, in Meisenheimer K., Röser H.-J., eds, *Hotspots in Extragalactic Radio Sources*, Springer-Verlag, Heidelberg, p. 27

Laing R.A., Jenkins C.R., Wall J.V., Unger S.W., 1994, in Bicknell G.V., Dopita M.A., Quinn P.J., eds, *The First Stromlo Symposium: the Physics of Active Galaxies*, ASP Conference Series vol. 54, San Francisco, p. 201 [L94]

Laing R.A., Peacock J.A., 1980, MNRAS, 190, 903

Laing R.A., Riley J.M., Longair M.S., 1983, MNRAS, 204, 151 [LRL]

LaValley M., Isobe T., Feigelson E.D., 1992, BAAS, 24, 839

Law-Green J.D.B., Leahy J.P., Alexander P., Allington-Smith J.R., van Breugel W.J.M., Eales S.A., Rawlings S.G., Spinrad H., 1995, MNRAS, 274, 939

Leahy J.P., Black A.R.S., Dennett-Thorpe J., Hardcastle M.J., Komissarov S., Perley R.A., Riley J.M., Scheuer P.A.G., 1997, MNRAS, 291, 20 [L97]

Leahy J.P., Perley R.A., 1991, AJ, 102, 527

Leahy J.P., Perley R.A., 1995, MNRAS, 277, 1097

Morganti R., Oosterloo T.A., Fosbury R.A.E., Tadhunter C.N., 1995, MNRAS, 274, 393

Morganti R., Oosterloo T.A., Reynolds J.E., Tadhunter C.N., Migenes V., 1997, MNRAS, 284, 541

Orr M.J.L., Browne I.W.A., 1982, MNRAS, 200, 1067

Osterbrock D.E., Miller J.S., 1975, ApJ, 197, 535

Parma P., Fanti C., Fanti R., Morganti R., De Ruiter H.R., 1987, A&A, 181, 244

Perley R.A., Dreher J.W., Cowan J.J., 1984, ApJ, 285, L35

Roettiger K., Burns J.O., Clarke D.A., Christiansen W.A., 1994, ApJ, 421, L23

Ryle M., Longair M.S., 1967, MNRAS, 136, 123

Sargent W.L.W., 1977, ApJ, 212, L105

Scheuer P.A.G., 1987, in Zensus J., Pearson T., eds, *Superluminal Radio Sources*, Cambridge University Press, Cambridge, p. 104

Simpson C., Ward M., Clements D.L., Rawlings S., 1996, MNRAS, 281, 509

Smith H.E., Spinrad H., Smith E.O., 1976, PASP, 88, 621

Spangler S.R., Myers S.T., Pogge J.J., 1984, AJ, 89, 1478

Spencer R.E., Schilizzi R.T., Fanti C., Fanti R., Parma P., van Breugel W.J.M., Venturi T., Muxlow T.W.B., Rendong N., 1991, MNRAS, 250, 225

Stull M.A., 1971, AJ, 76, 1

Swain M.R., Bridle A.H., Baum S.A., 1996, in Hardee P.E., Bridle A.H., Zensus J.A., eds, *Energy Transport in Radio Galaxies and Quasars*, ASP Conference Series vol. 100, San Francisco, p. 299

Tadhunter C.N., Morganti R., di Serego Alighieri S., Fosbury R.A.E., Danziger I.J., 1993, MNRAS, 263, 999

van Breugel W., Miley G., Heckman T., Butcher H., Bridle A., 1985, ApJ, 290, 496

van Breugel W.J.M., Dey A., 1993, ApJ, 414, 563

Wardle J.F.C., Aaron S.E., 1997, MNRAS, 286, 425

Yee H.K.C., Oke J.B., 1978, ApJ, 226, 753

Zirbel E.L., Baum S.A., 1995, ApJ, 448, 521

Table 1. The combined sample of FRII radio sources

Source	IAU name	z	S_{178} (Jy)	α	P_{178}	LAS (arcsec)	Size (kpc)	Jets?	Ref.	Freq. (GHz)	Emission class
4C 12.03	0007+124	0.156	10.9	0.87	104	215	787	oo	(9)	–	E
3C 15	0034–014	0.0730	17.2	0.67	33	48.0	92	••	2	8.4	E
3C 20	0040+517	0.174	46.8	0.66	543	53.6	214	oo	1	8.4	N
3C 33	0106+130	0.0595	59.3	0.76	75	254	404		(9)	–	N
3C 33.1	0106+729	0.181	14.2	0.62	178	227	935	•	11	1.5	B
3C 61.1	0210+860	0.186	34.0	0.77	462	186	782	o	(12)	–	N
3C 79	0307+169	0.2559	33.2	0.92	930	89.0	474		1	8.4	N
3C 98	0356+109	0.0306	51.4	0.78	17	310	264	•	2	8.4	N
3C 105	0404+035	0.089	19.4	0.61	56	335	764	o	2	8.4	N
4C 14.11	0411+141	0.206	12.1	0.84	208	116	527	•	1	8.4	E
3C 111	0415+379	0.0485	70.4	0.76	59	215	283	•	2	8.4	B
3C 123	0433+295	0.2177	206.0	0.70	3873	37.8	179		1	8.4	E
3C 132	0453+227	0.214	14.9	0.68	269	22.4	105	o	1	8.4	E
3C 135	0511+008	0.1273	18.9	0.95	118	132	409	•	2	8.4	N
3C 136.1	0512+248	0.064	15.3	0.72	22	460	781		2	8.4	?
3C 153	0605+480	0.2771	16.7	0.66	524	9.1	51	oo	1	8.4	N
3C 171	0651+542	0.2384	21.3	0.87	505	32.5	165	••	1	8.1	N
3C 173.1	0702+749	0.292	16.8	0.88	624	60.5	353	•	1	8.4	E
3C 184.1	0734+805	0.1182	14.2	0.68	73	182	530	o	2	8.4	N
3C 192	0802+243	0.0598	23.0	0.79	29	200	319	o	2	8.4	N
3C 197.1	0818+472	0.1301	8.8	0.72	56	24.0	76		3	8.4	E
3C 219	0917+458	0.1744	44.9	0.81	536	190	760	•o	10	4.9	B
3C 223	0936+361	0.1368	16.0	0.74	113	306	1007	oo	2	8.4	N
3C 223.1	0938+399	0.1075	8.1	0.73	35	140	376	o	3	8.4	N
3C 227	0945+076	0.0861	33.1	0.70	89	230	510		3	8.4	B
3C 234	0958+290	0.1848	34.2	0.86	466	112	469	•	1	8.4	N
3C 277.3	1251+278	0.0857	9.8	0.58	26	49.0	108	•	(14)	–	E
3C 284	1308+277	0.2394	12.3	0.95	299	178	904		1	8.1	N
3C 285	1319+428	0.0794	12.3	0.95	29	180	371	oo	7	4.9	N
3C 300	1420+198	0.272	19.5	0.78	604	100	561	•	1	8.1	N
3C 303	1441+522	0.141	12.2	0.76	92	47.0	159	•	9	1.5	B
3C 319	1522+546	0.192	16.7	0.90	249	105	453		1	8.4	E
3C 321	1529+242	0.096	14.7	0.60	49	307	748	•	(2)	–	N
3C 327	1559+021	0.1039	38.5	0.64	152	302	788	oo	2	8.4	N
3C 349	1658+471	0.205	14.5	0.74	242	85.9	389	o	1	8.4	N
3C 353	1717+009	0.0304	257.2	0.74	83	284	240	••	8	8.4	E
3C 381	1832+474	0.1605	18.1	0.81	181	73.2	274		1	8.4	B
3C 382	1833+326	0.0578	21.7	0.59	26	185	286	•	3	8.4	B
3C 388	1842+455	0.0908	26.8	0.70	81	50.0	116	oo	5	4.9	E
3C 390.3	1845+797	0.0561	51.8	0.75	58	229	345	oo	4	8.4	B
3C 401	1939+605	0.201	22.8	0.71	362	23.6	105	•	1	8.4	E
3C 403	1949+023	0.059	28.3	0.74	35	230	362	•	3	8.4	N
3C 405	1957+405	0.0565	9660.0	0.74	11001	130	197	••	6	4.5	N
3C 424	2045+068	0.127	15.9	0.88	98	35.0	108	•	3	8.4	E
3C 430	2117+605	0.0541	36.7	0.75	38	90.0	131		(13)	–	E
3C 433	2121+248	0.1016	61.3	0.75	233	68.0	174	•	3	8.4	N
3C 436	2141+279	0.2145	19.4	0.86	365	109	511	•	1	8.4	N
3C 438	2153+377	0.290	48.7	0.88	1783	22.6	131	••	1	8.4	E
3C 445	2221–021	0.0562	27.0	0.76	30	570	859	oo	2	8.4	B
3C 452	2243+394	0.0811	59.3	0.78	142	280	588	••	3	8.4	N

Objects whose names are in bold face are drawn from the complete sample of LRL. Column 4 gives the 178-MHz flux density of the source. Column 5 gives the low-frequency (178–750 MHz) spectral index. Column 6 gives the luminosity at 178 MHz; the units are 10^{24} W Hz $^{-1}$ sr $^{-1}$. Column 7 gives largest angular size, measured from the best available maps. Column 9 gives information on jet detection. A filled circle indicates a definite jet and an open circle a possible jet. Column 10 gives references to maps used, as follows: (1) H97 and references therein. (2) L97. (3) B92; Black (1992). (4) Dennett-Thorpe (1996). (5) Roettiger et al. (1994). (6) Perley, Dreher & Cowan (1984) (7) van Breugel & Dey (1993). (8) Swain, Bridle & Baum (1996). (9) Leahy & Perley (1991). (10) Clarke et al. (1992). (11) Leahy, in preparation. (12) Alexander (1985). (13) Spangler, Myers & Pogge (1984). (14) van Breugel et al. (1985). References in parentheses are to papers used to classify the jets of objects that were not included in the analysis. Column 11 gives the observing frequency of the map used. Column 12 gives the emission line type of the source: ‘E’ indicates a LERG, ‘N’ a NLRG and ‘B’ a BLRG; ‘?’ indicates an unclassified source. These mostly reflect classifications in LRL, supplemented by references quoted in H97, or from the spectrophotometry of Laing and co-workers (L94; Laing, private communication) for sources in LRL. The non-LRL sources have been classified from the following literature: 3C 15, 3C 105, 3C 403, Tadhunter et al. (1993); 3C 111, Sargent (1977); 3C 135, 3C 445, Eracleous & Halpern (1994); 3C 227, 3C 327, 3C 353, Simpson et al. (1996); 3C 197.1, 3C 424 (tentatively), 3C 430, Smith, Spinrad & Smith (1976); 3C 223.1, Cohen & Osterbrock (1981); 3C 277.3, Yee & Oke (1978); 3C 405, Osterbrock & Miller (1975). 3C 136.1 has strong emission lines (Smith et al. 1976) but is not classified as broad or narrow-line in the literature.

Table 2. Basic measured quantities

Source	Frequency (GHz)	Total flux density (Jy)	Error	Core flux density (mJy)	Error
3C 15	8.35	1.00		27.99	0.05
3C 20	8.44	2.29		3.32	0.06
3C 33.1	1.53	3.02		20.40	0.07
3C 79	8.44	0.694		6.04	0.01
3C 98	8.35	3.08	0.07	6.1	0.1
3C 105	8.35	1.68		18.9	0.5
4C 14.11	8.44	0.500		29.69	0.03
3C 111	8.35	4.8	0.2	1276	1
3C 123	8.44	9.44		108.9	0.3
3C 132	8.44	0.674		4.1	0.2
3C 135	8.35	0.520		1.0	0.2
3C 136.1	8.35	1.00	0.05	1.53	0.03
3C 153	8.44	0.712		< 0.5	
3C 171	8.06	0.690		2.0	0.1
3C 173.1	8.44	0.461		9.64	0.02
3C 184.1	8.35	0.785		6.0	0.5
3C 192	8.35	1.38	0.08	4.0	0.2
3C 197.1	8.35	0.320		6.0	0.1
3C 219	4.87	2.27	0.06	51.6	0.1
3C 223	8.35	0.89	0.05	8.5	0.2
3C 223.1	8.35	0.53	0.01	6.4	0.4
3C 227	8.35	2.05	0.04	13.2	0.6
3C 234	8.44	0.919		34.46	0.04
3C 284	8.06	0.340		2.79	0.02
3C 285	4.86	0.740		6.8	0.4
3C 300	8.06	0.645		6.2	0.1
3C 303	1.48	2.45		106.6	0.3
3C 319	8.44	0.362		< 0.3	
3C 327	8.35	2.01	0.05	25	1
3C 349	8.44	0.723		24.21	0.02
3C 353	8.44	14.1		151.0	0.2
3C 381	8.44	0.906		4.7	0.1
3C 382	8.35	1.30		251.2	0.1
3C 388	4.87	1.80		57.9	0.1
3C 390.3	8.35	2.8	0.1	733	5
3C 401	8.44	0.844		28.54	0.03
3C 403	8.35	1.50		7.1	0.2
3C 405	4.53	415		776	3
3C 424	8.35	0.357		7.0	0.3
3C 433	8.35	2.08		1.2	0.3
3C 436	8.44	0.592		17.90	0.02
3C 438	8.44	0.780		16.2	0.1
3C 445	8.40	1.34	0.08	83.9	0.4
3C 452	8.35	2.14		125.8	0.3

The total flux densities for 3C 98, 3C 136.1, 3C 192, 3C 227, 3C 327 and 3C 445 are taken from the single-dish measurements of Stull (1971), as these sources were all seriously undersampled by the VLA observations. These numbers are to be treated with caution. Stull's flux scale is not consistent with that of Baars et al. (1977), but the systematic error is much less than 1 per cent. The random error due to the calibration process is tabulated above and is as given by Stull. In addition, the flux densities have not been corrected from 8.0 GHz to the VLA frequency, which makes them systematically high by up to 5 per cent. The 5-GHz flux density of 3C 219 is from Laing & Peacock (1980). The flux densities for 3C 223 and 3C 390.3 were interpolated from other frequencies, and the errors assigned to them are estimates of the error in the interpolation. Elsewhere errors are only assigned where the integration was problematic because of off-source noise, but the VLA calibration errors apply in addition to these and to any source with no error assigned. Noise or mild undersampling means that the flux densities of 3C 105, 3C 111, 3C 132, 3C 171, 3C 197.1, 3C 284 and 3C 382 may be too low. The flux density of 3C 303 is taken from Leahy & Perley (1991). The core flux densities of 3C 79, 4C 14.11, 3C 111 and 3C 390.3 are variable (see H97, L97 and Leahy & Perley 1995). We took the southern component of 3C 424's core to be the true core (*pace* B92).

Table 3. Flux densities and sizes of lobes

Source	Frequency (GHz)	North lobe			South lobe		
		Flux density (Jy)	Error	Length (arcsec)	Flux density (Jy)	Error	Length (arcsec)
3C 15	8.35	0.54	0.01	24.6	0.41	0.01	23.6
3C 20	8.44	1.23	0.02	27.2	1.06	0.02	28.7
3C 33.1	1.53	1.73	0.02	87.9	1.28	0.02	152
3C 79	8.44	0.386		38.3	0.302		50.8
3C 98	8.35	1.67		138	1.44		178
3C 105	8.35	0.356		162	1.31		171
4C 14.11	8.44	0.231	0.005	58.6	0.239	0.005	57.5
3C 111	8.35	–		123	–		93.9
3C 123	8.44	3.31		19.2	6.02		17.6
3C 132	8.44	0.273	0.005	11.7	0.397	0.005	11.0
3C 135	8.35	0.186	0.005	78.8	0.337	0.005	51.7
3C 136.1	8.35	–		191	–		267
3C 153	8.44	0.355	0.002	4.3	0.356	0.002	4.8
3C 171	8.06	0.386		24.4	0.302		12.1
3C 173.1	8.44	0.201		27.2	0.250		33.4
3C 184.1	8.35	0.397	0.001	107	0.382	0.001	82.0
3C 192	8.35	–		109	–		93.0
3C 197.1	8.35	0.147	0.005	16.0	0.170	0.005	11.6
3C 219	4.87	–		97.8	–		92.1
3C 223	8.35	0.440		156	0.320		152
3C 223.1	8.35	0.180		81.0	0.215		60.0
3C 227	8.35	1.03		113	0.660		121
3C 234	8.44	0.334	0.005	64.6	0.551	0.005	48.0
3C 284	8.06	0.152	0.003	106	0.185	0.003	72.6
3C 285	4.86	0.408		87.0	0.325		103
3C 300	8.06	0.154	0.005	70.2	0.485	0.005	31.8
3C 303	1.48	1.90	0.02	27.8	0.40	0.01	20.8
3C 319	8.44	0.25	0.01	48.9	0.12	0.01	57.9
3C 327	8.35	–		199	–		108
3C 349	8.44	0.269	0.008	41.7	0.430	0.008	44.2
3C 353	8.44	8.5	0.1	142	5.5	0.1	142
3C 381	8.44	0.570		33.2	0.331		40.0
3C 382	8.35	0.790		87.9	0.580		91.0
3C 388	4.87	0.869		27.9	0.873		22.5
3C 390.3	8.35	–		132	–		92.0
3C 401	8.44	0.348	0.005	10.7	0.467	0.005	12.9
3C 403	8.35	–		95.0	–		116
3C 405	4.53	205		70.6	209		60.6
3C 424	8.35	0.120	0.005	13.0	0.230	0.005	21.0
3C 433	8.35	0.237	0.005	41.0	1.84	0.01	32.5
3C 436	8.44	0.27	0.01	59.2	0.30	0.01	49.6
3C 438	8.44	0.368	0.005	11.9	0.397	0.005	10.8
3C 445	8.40	–		299	–		280
3C 452	8.35	0.940		141	1.07		135

Flux densities are listed only where maps were available to us that appeared to reproduce the large-scale structure well. Errors have been assigned where there was some difficulty in separating the north and south lobes, and so where some flux might be assigned to either; the errors are rough estimates of the variation over multiple attempts at integration. These are in addition to the errors due to VLA flux calibration, which apply to all the measurements. Lengths are measured from the core to the most distant visible region of emission. In several cases these lengths are measured substantially away from the source axis: these, with their on-axis lengths in parentheses, are 3C 105N (156 arcsec), 3C 171N (5.0) and S (4.8), 3C 197.1N (7), 3C 300S (30), 3C 403N (55.5) and S (52.8) and 3C 433N (24.6).

Table 4. Flux densities and lengths of jets

Source	Freq. (GHz)	North jet			South jet		
		Flux density (mJy)	Error	Length	Flux density (mJy)	Error	Length
3C 15	8.35	210	10	9.50	3.6	0.9	6.20
3C 20	8.44	23	6	18.3	*3.7	0.9	6.80
3C 33.1	1.53	< 56			170	10	78.0
3C 79	8.44	< 3.8			< 1.3		
3C 98	8.35	90	20	121	< 0.79		
3C 105	8.35	< 8.3			*40	10	17.2
4C 14.11	8.44	< 2.5			1.9	0.3	2.80
3C 111	8.35	100	10	114	< 2.8		
3C 123	8.44	< 2.1			< 30		
3C 132	8.44	< 7.2			*3	2	5.97
3C 135	8.35	< 3			3.1	0.4	21.4
3C 136.1	8.35	< 2.6			< 2.7		
3C 153	8.44	*1.9	0.6	1.20	*13	2	1.40
3C 171	8.06	15	1	3.80	6.3	0.9	3.50
3C 173.1	8.44	2.4	0.8	10.2	< 2.4		
3C 184.1	8.35	*14	3	32.2	< 1.3		
3C 192	8.35	< 3.2			*8	1	13.9
3C 197.1	8.35	< 1.9			< 0.85		
3C 219	4.87	*2.09	0.09	1.40	56.1	0.5	16.5
3C 223	8.35	*8	2	29.4	*5	9	42.0
3C 223.1	8.35	*2.5	0.7	19.2	< 7.7		
3C 227	8.35	< 15			< 27		
3C 234	8.44	3	2	6.20	< 2.3		
3C 284	8.06	< 2.8			< 6.6		
3C 285	4.86	36	7	74.6	< 2.1		
3C 300	8.06	38	4	62.6	< 1.7		
3C 303	1.48	66	4	14.2	< 7.4		
3C 319	8.44	< 0.12			< 1.8		
3C 327	8.35	*11	3	107	*11	3	60.4
3C 349	8.44	< 2.1			*0.24	0.04	1.10
3C 353	8.44	90	10	71.0	30	8	37.0
3C 381	8.44	< 2.9			< 1.3		
3C 382	8.35	31	2	77.9	< 0.14		
3C 388	4.87	*10	2	4.58	49	8	12.7
3C 390.3	8.35	34	5	81.3	*2	1	21.0
3C 401	8.44	< 4			114	9	5.85
3C 403	8.35	7.8	0.6	24.0	—		
3C 405	4.53	2300	300	50.3	380	40	24.1
3C 424	8.35	< 11			15	1	3.04
3C 433	8.35	47	9	24.1	< 1.4		
3C 436	8.44	< 0.51			19	3	38.8
3C 438	8.44	43	9	8.90	40	3	7.40
3C 445	8.40	*1.3	0.3	5.60	10.3	0.7	60.0
3C 452	8.35	16	3	95.4	31	7	108

Flux densities of jets classed as ‘possible’ in Table 1 are marked with an asterisk.

Table 5. Flux densities and lengths of straight jets

Source	Freq. (GHz)	North straight jet		South straight jet		Length
		Flux density (mJy)	Error	Flux density (mJy)	Error	
3C 15	8.35	96	3	< 1.4		4.17
3C 20	8.44	7	5	* < 9		12.4
3C 33.1	1.53	< 37		27	4	51.0
3C 79	8.44	–		–		
3C 98	8.35	50	20	< 13		101
3C 105	8.35	–		–		
4C 14.11	8.44	< 0.45		1.14	0.04	15.0
3C 111	8.35	90	20	< 58		101
3C 123	8.44	–		–		
3C 132	8.44	< 13		* 2	3	5.00
3C 135	8.35	< 1.6		10	4	30.2
3C 136.1	8.35	–		–		
3C 153	8.44	* 8	1	* 13	5	1.70
3C 171	8.06	6.0	0.7	6.3	0.8	3.07
3C 173.1	8.44	2.1	0.9	< 0.29		11.2
3C 184.1	8.35	–		–		
3C 192	8.35	–		–		
3C 197.1	8.35	–		–		
3C 219	4.87	* 56.5	0.3	2.1	0.1	17.1
3C 223	8.35	* 11	4	* < 5.8		34.1
3C 223.1	8.35	* 3	1	< 21		21.9
3C 227	8.35	–		–		
3C 234	8.44	10	8	< 19		59.1
3C 284	8.06	–		–		
3C 285	4.86	19	2	< 14		51.6
3C 300	8.06	2.4	0.2	< 0.23		4.70
3C 303	1.48	63	5	< 13		12.3
3C 319	8.44	–		–		
3C 327	8.35	* 16	6	* < 140		119
3C 349	8.44	< 0.053		* 0.31	0.04	1.27
3C 353	8.44	70	10	< 34		66.5
3C 381	8.44	–		–		
3C 382	8.35	14	1	< 1.1		48.3
3C 388	4.87	* 30	5	34	6	8.40
3C 390.3	8.35	20	10	* < 650		88.6
3C 401	8.44	< 5.7		33.8	0.4	5.67
3C 403	8.35	6	1	< 3.8		19.6
3C 405	4.53	1200	600	500	800	40.8
3C 424	8.35	< 8.4		16.7	0.9	2.99
3C 433	8.35	9.8	0.1	< 8.3		4.43
3C 436	8.44	< 0.27		3.8	0.8	20.2
3C 438	8.44	40	4	< 9.8		8.67
3C 445	8.40	* < 1.9		14	3	78.1
3C 452	8.35	9	2	13	2	46.4

Flux densities of jets classed as ‘possible’ in Table 1 are marked with an asterisk.

Table 6. Flux densities and sizes of hot spots

Source	Freq. (GHz)	Flux density (mJy)	North hot spot				South hot spot				
			Error	θ_{maj}	θ_{min}	Dist.	Flux density (mJy)	Error	θ_{maj}	θ_{min}	
3C 15	8.35	—	—	—	—	—	*5	1	1.5	1.0	18.2
3C 20	8.44	160	10	0.21	0.16	24.1	89	2	0.22	0.18	23.3
3C 79	8.44	4	1	0.21	0.08	36.8	15	2	0.53	0.34	50.4
3C 98	8.35	*40	10	4.1	3.4	132	27	5	3.9	2.0	155
3C 105	8.35	3.2	0.6	1.7	0.80	155	110	5	0.28	0.20	171
4C 14.11	8.44	1.7	0.5	1.2	0.10	58.1	3.3	0.1	0.29	0.09	36.4
3C 111	8.35	300	10	1.3	0.70	123	76	1	1.9	1.1	74.1
3C 123	8.44	21	2	0.15	0.08	7.3	162	5	0.11	0.08	7.9
3C 132	8.44	53	1	0.19	0.15	11.3	22	4	0.40	0.25	10.9
3C 135	8.35	1.7	0.2	0.55	0.25	72.3	*77	5	4.6	1.7	45.0
3C 136.1	8.35	*56	8	20	10	173	*23	5	12	12	255
3C 153	8.44	133	2	0.19	0.08	2.4	87	1	0.11	0.07	4.8
3C 171	8.06	120	10	0.27	0.07	4.9	95	2	0.29	0.19	4.6
3C 173.1	8.44	8.3	0.3	0.47	0.18	26.4	10	2	0.50	0.25	31.9
3C 184.1	8.35	*7	2	2.6	1.0	103	19	1	0.95	0.50	78.2
3C 192	8.35	*80	20	4.0	3.0	103	2.0	0.2	1.2	0.90	88.5
3C 197.1	8.35	3.4	0.1	0.33	0.30	6.8	8.5	0.5	0.75	0.35	9.6
3C 219	4.87	2.9	0.2	0.99	0.36	72.6	76	1	3.2	1.6	73.1
3C 223	8.35	10	1	3.5	1.3	140	*6	2	6.0	2.0	147
3C 223.1	8.35	*14	4	2.0	0.80	40.3	13	1	0.90	0.40	38.5
3C 227	8.35	17	1	0.90	0.60	108	*7	1	1.0	0.50	109
3C 234	8.44	55.8	0.1	0.51	0.20	63.9	50	10	0.73	0.35	47.4
3C 284	8.06	*6	2	1.5	0.75	104	27	2	0.76	0.57	72.4
3C 285	4.86	*4	1	3.0	2.0	78.8	*4	1	9.0	7.0	92.5
3C 300	8.06	*1.0	0.5	0.30	0.30	69.7	29	1	0.44	0.26	29.3
3C 303	1.48	650	10	< 1.7	1.1	16.9	5.0	0.5	0.90	0.50	16.9
3C 319	8.44	19	3	1.4	0.90	47.7	—	—	—	—	—
3C 327	8.35	3.5	0.2	0.40	0.30	182	20	1	1.0	0.35	99.1
3C 349	8.44	*4	1	0.50	0.30	40.3	90	5	0.65	0.47	42.9
3C 353	8.44	*70	10	4.5	2.5	94.4	63	2	3.2	1.8	123
3C 381	8.44	9	1	0.20	0.17	32.5	*7	2	0.80	0.40	35.5
3C 382	8.35	45	5	2.2	2.0	86.5	*8	2	2.3	2.1	82.4
3C 388	4.87	40	10	2.8	1.6	15.9	55	2	1.2	0.90	16.4
3C 390.3	8.35	67	2	2.5	1.2	104	450	20	4.1	2.0	88.4
3C 401	8.44	*5	2	0.50	0.50	8.8	*4	2	0.60	0.20	12.3
3C 403	8.35	30	1	0.40	0.21	28.5	*20	10	4.0	0.90	47.8
3C 405	4.53	3060	20	0.61	0.35	63.2	2320	50	1.0	0.47	53.1
3C 424	8.35	2.7	0.2	0.20	0.15	8.7	24	2	0.50	0.20	4.2
3C 433	8.35	—	—	—	—	—	*6	2	0.65	0.55	0.0
3C 436	8.44	*2	1	2.2	1.0	57.4	11	1	0.34	0.21	43.5
3C 438	8.44	*4	2	0.30	0.10	11.4	*2	1	0.30	0.10	8.9
3C 445	8.40	43	2	2.2	1.0	291	60	10	3.7	1.4	275
3C 452	8.35	*20	10	3.5	1.2	130	31	1	1.0	0.84	126

θ_{maj} , θ_{min} and ‘Dist.’ are in arcseconds. ‘Dist.’ is the distance between the hot spot and the core. Flux densities marked with an asterisk were measured by integration, and their associated major and minor axes (θ_{maj} and θ_{min}) by estimation from the maps rather than by using Gaussian fitting. In several cases it was not clear which object was the primary; in these cases fits were made to each candidate component and the results for the most compact components were used here. The relevant objects are 3C 173.1N (N4 was used rather than N3), 3C 227N (F1a of B92 was used) 3C 285N (southern candidate object was preferred), 3C 300S (E2 was used rather than E3) and 3C 403N (F6 of B92 was taken to be the primary rather than F1). 3C 33.1 is omitted, as the maps available to us were not high enough in resolution to allow a measurement.

Table 7. Median values of important quantities

Quantity	All radio galaxies	NLRG	BLRG	NLRG and BLRG	LERG	B94 quasars
z	0.129 (0.182)	0.123 (0.179)	0.086 (0.150)	0.118 (0.167)	0.197 (0.210)	0.768
178-MHz luminosity (10^{24} W Hz $^{-1}$ sr $^{-1}$)	115 (237)	151 (241)	89 (134)	129 (181)	103 (268)	6600
Linear size (kpc)	367 (380)	409 (468)	344 (315)	406 (404)	130 (179)	418
Hot spot size (kpc)	2.42 (2.42)	2.38 (2.57)	3.32 (2.89)	2.49 (2.92)	2.15 (2.15)	–
Core prominence	0.012 (0.014)	0.0087 (0.0087)	0.067 (0.12)	0.011 (0.010)	0.021 (0.023)	0.062
Straight jet prominence	0.0064 (0.0067)	0.0055 (0.0057)	0.011 (0.011)	0.0067 (0.0069)	0.0049 (0.0042)	0.0088
Total jet prominence	0.014 (0.018)	0.013 (0.018)	0.026 (0.029)	0.017 (0.019)	0.0063 (0.0051)	0.053

Values in parentheses are drawn from the sub-sample of objects taken from LRL (which constitute a flux-limited sample).

Table 8. Summary of trends and correlations

Proposition tested	Significant?
LERG are smaller than NLRG and BLRG	Y (99.9 per cent)
BLRG are smaller than NLRG	N
Hot spot size is correlated with total linear size	Y (99.9 per cent)
The brighter jet points towards the more compact hot spot	N
The hot spot on the jetted size is less recessed	Y? (90 per cent)
The brighter jet points towards the brighter hot spot	Y? (90 per cent)
LERG are less symmetrical than NLRG	N
BLRG are more symmetrical than NLRG	Y (97 per cent)
Jet prominence depends on luminosity	N
Jet detection fraction depends on emission line class	N
BLRG straight jets are more prominent than NLRG straight jets	Y (95 per cent)
B94 quasar total jets are more prominent than BLRG total jets	Y (95 per cent)
B94 quasar straight jets are more prominent than BLRG straight jets	N
Jets are preferentially detected in shorter objects	Y (90 per cent)
Brighter jets lie in longer lobes	N
Brighter jets lie in brighter lobes	N
Jet length is correlated with total linear size	Y (99 per cent)
BLRG cores are more prominent than NLRG cores	Y (99 per cent)
LERG cores and NLRG/BLRG cores are drawn from distributions with different medians	N
LERG cores and NLRG/BLRG cores are drawn from different distributions	Y? (90 per cent)
B94 quasar cores are more prominent than BLRG cores	N
NLRG core prominence is correlated with total linear size	Y (99 per cent)
Straight jet prominence is correlated with core prominence	Y (95 per cent)

Trends and correlations are considered significant (Y) if the probability of the observed result under the null hypothesis is ≤ 5 per cent, marginally significant (Y?) if it is ≤ 10 per cent and not significant (N) otherwise.

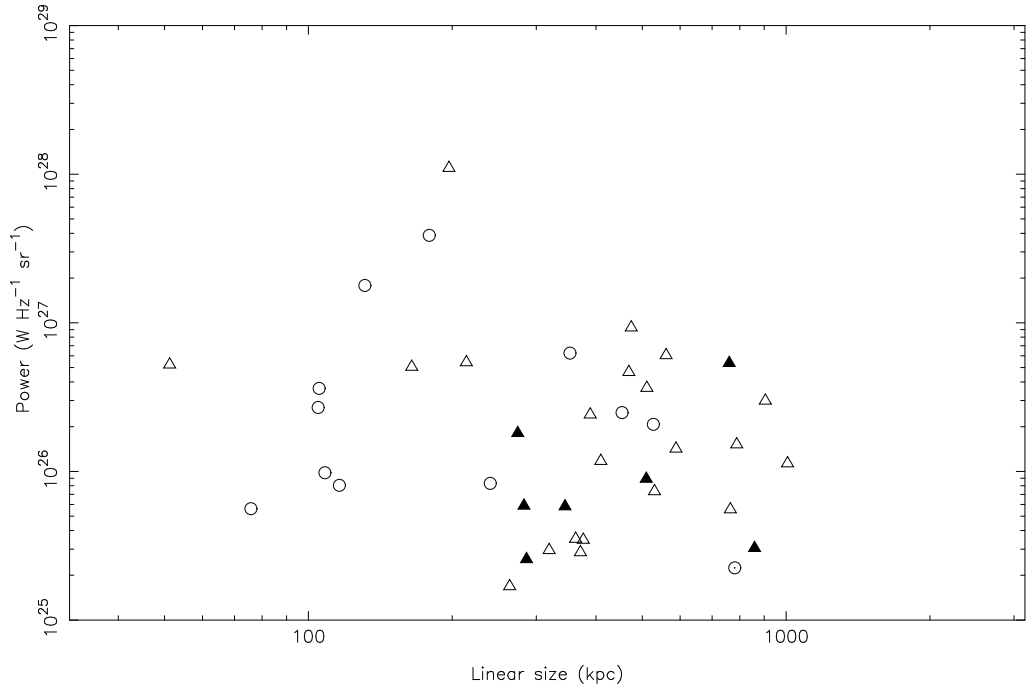


Figure 1. The power-linear-size diagram for the sample of radio sources. Open circles denote LERG; a dotted circle denotes an unclassified object; open triangles denote NLRG and filled triangles BLRG.

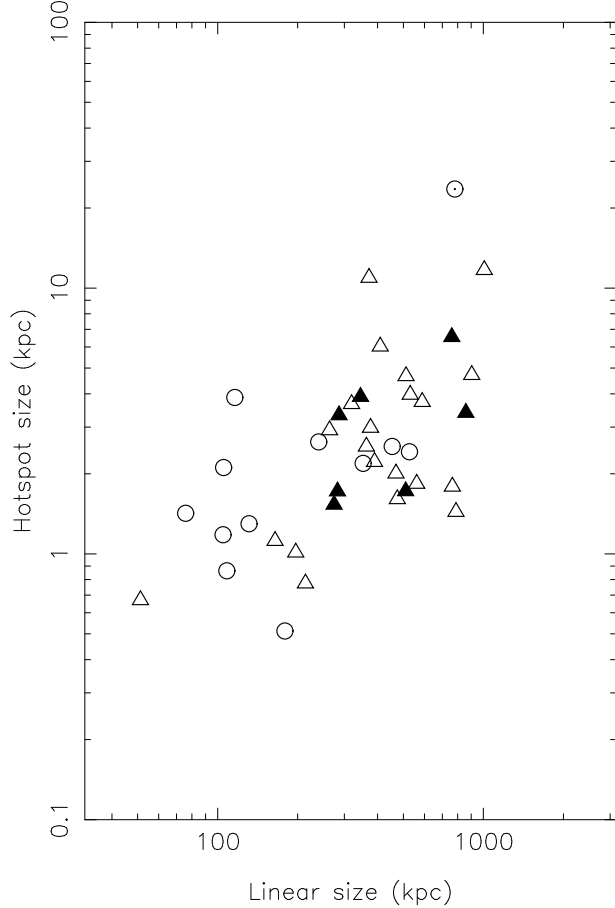


Figure 2. Linear sizes of the hot spots of the objects with good measurements against largest linear size. Open circles denote LERG; a dotted circle denotes an unclassified object; open triangles denote NLRG and filled triangles BLRG.

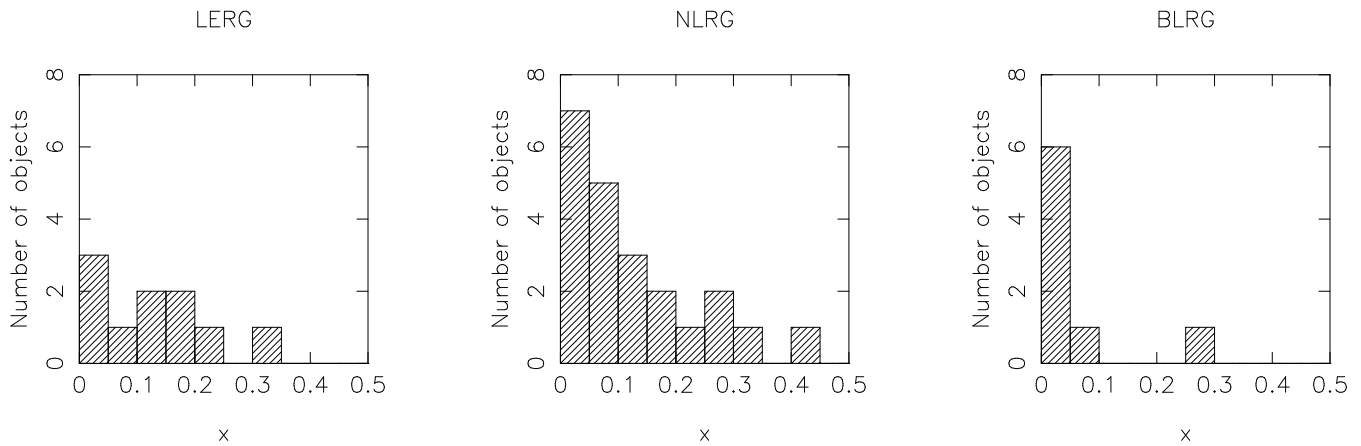


Figure 3. Histograms of the fractional separation parameter x for the sources with measured hot spot positions. The unclassified source is not plotted.

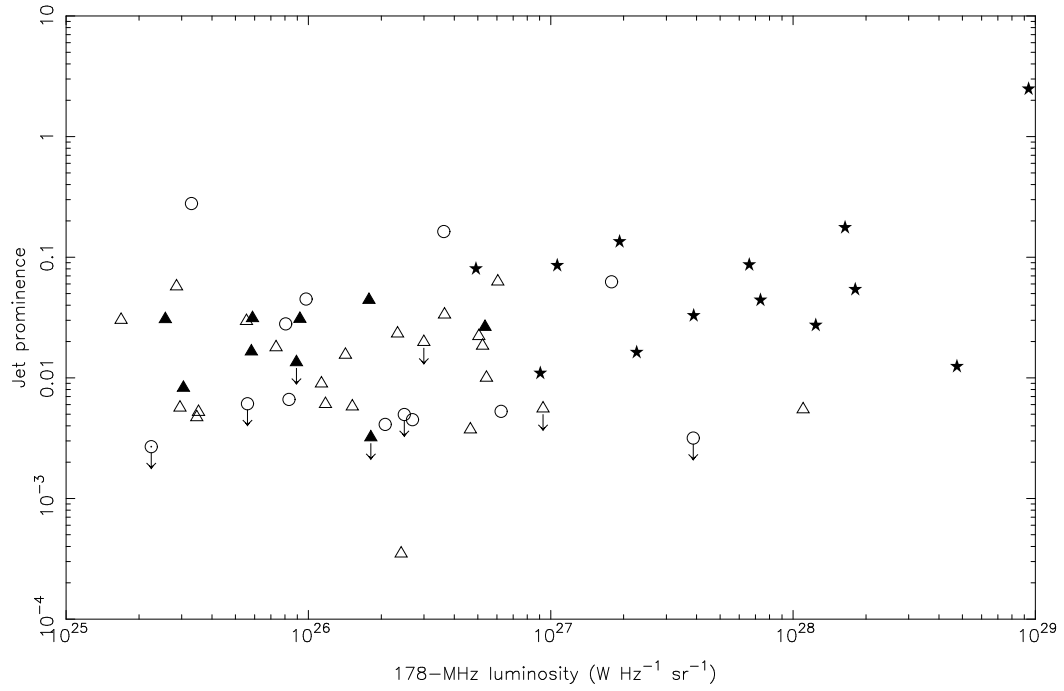


Figure 4. (Brighter) jet prominence against total low-frequency luminosity. Upper limits are marked with arrows. The radio galaxies are shown with the B94 quasars. Open circles denote LERG; a dotted circle denotes an unclassified object; open triangles denote NLRG and filled triangles BLRG; filled stars denote quasars.

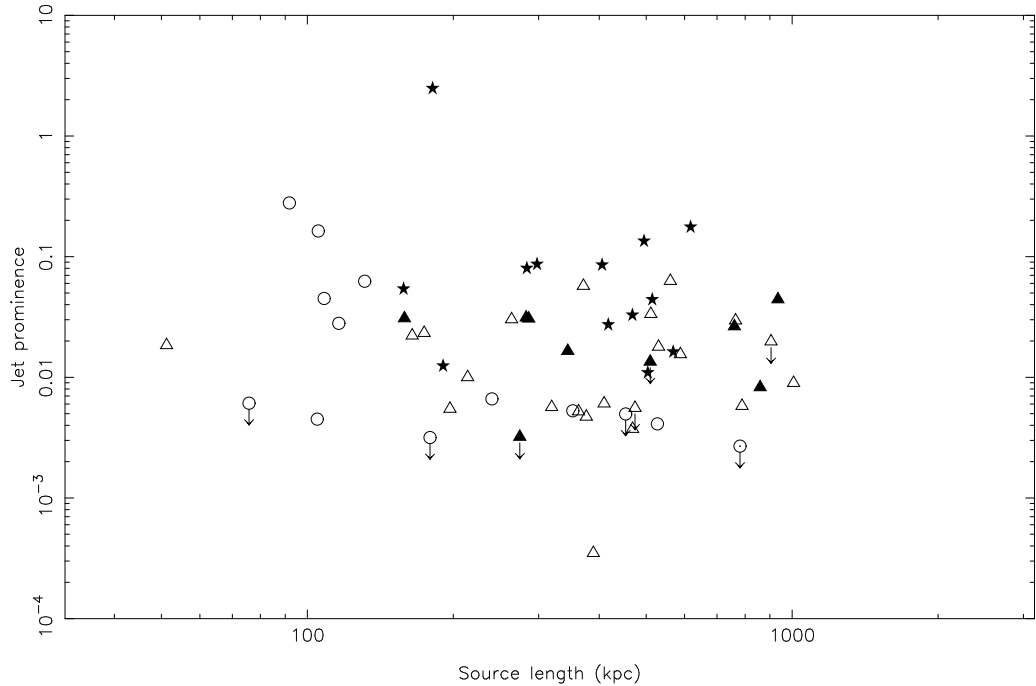


Figure 5. (Brighter) jet prominence against linear size. Upper limits are marked with arrows. The radio galaxies are shown with the B94 quasars. Open circles denote LERG; a dotted circle denotes an unclassified object; open triangles denote NLRG and filled triangles BLRG.

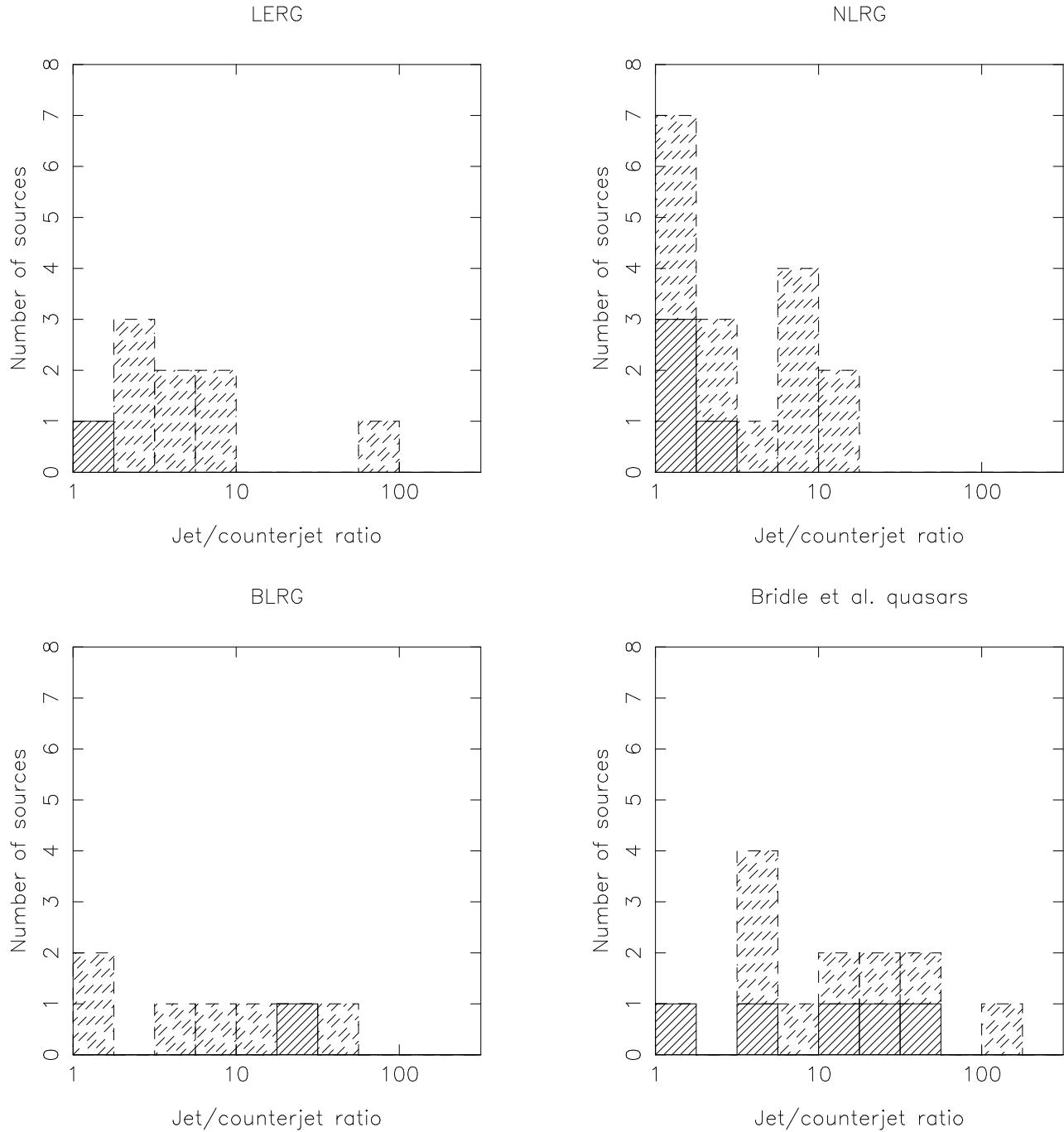


Figure 6. Jet sidedness of radio galaxies and quasars. Dashed shading indicates lower limits.

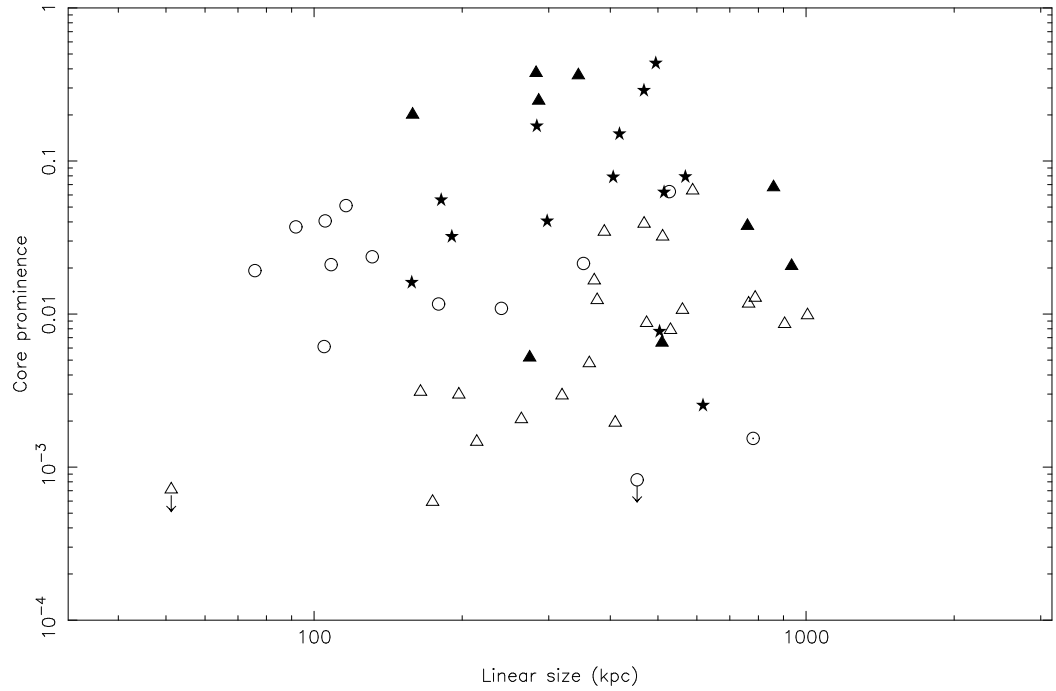


Figure 7. Core prominence as a function of source linear size. The radio galaxies are shown with the B94 quasars. Open circles denote LERG; a dotted circle denotes an unclassified object; open triangles denote NLRG and filled triangles BLRG; filled stars denote quasars.

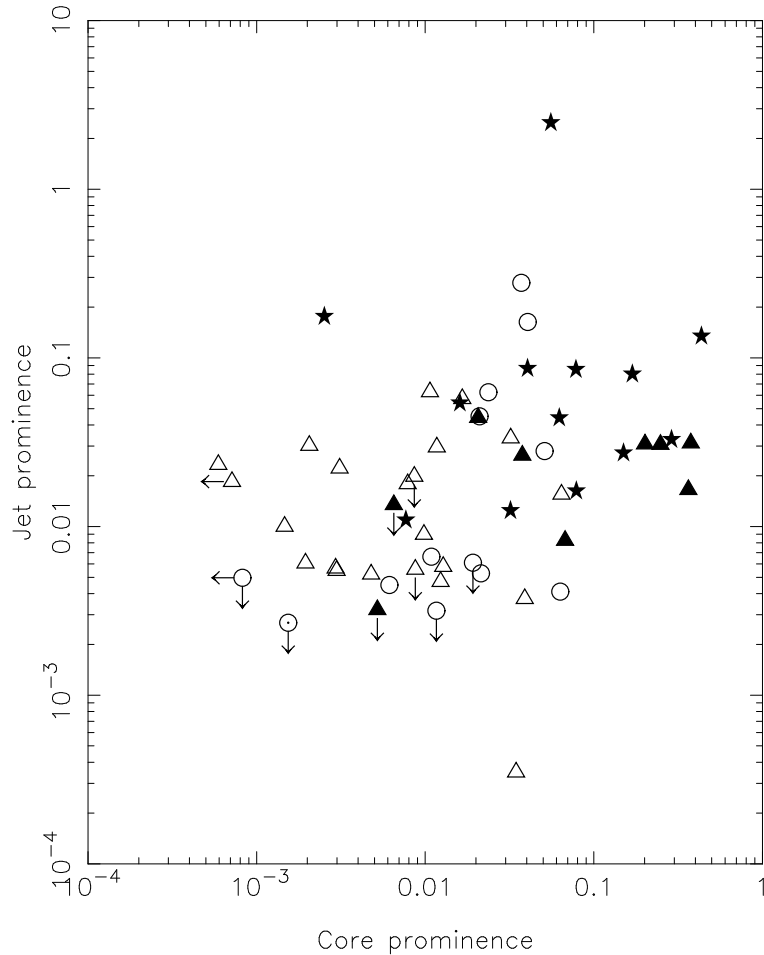


Figure 8. (Brighter) jet prominence as a function of core prominence. The radio galaxies are shown with the B94 quasars. Open circles denote LERG; a dotted circle denotes an unclassified object; open triangles denote NLRG and filled triangles BLRG; filled stars denote quasars.

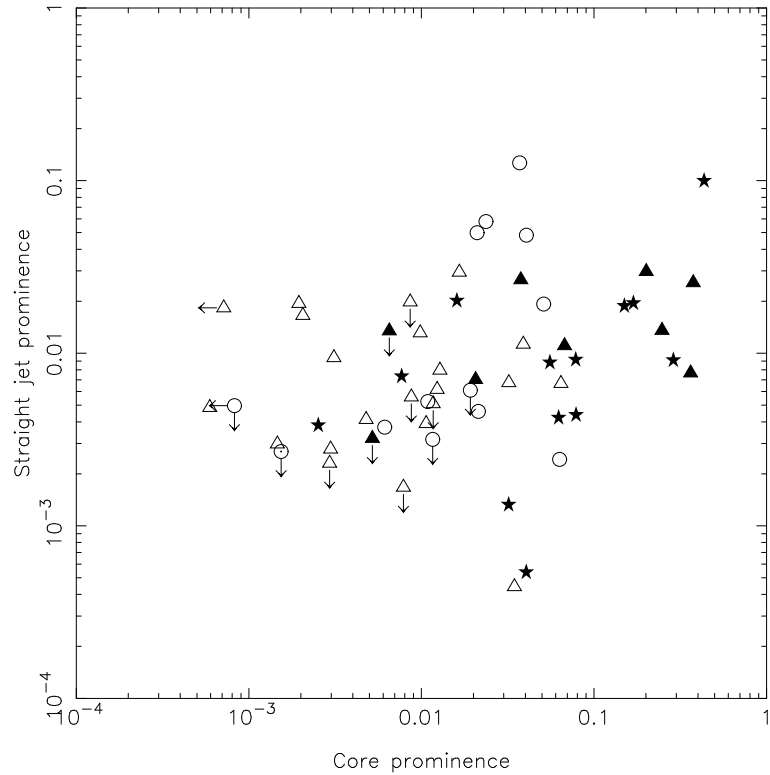


Figure 9. (Brighter) straight jet prominence against core prominence for the radio galaxies and B94 quasars. Upper limits are marked with arrows. Open circles denote LERG; a dotted circle denotes an unclassified object; open triangles denote NLRG and filled triangles BLRG; filled stars denote quasars.